

Improved ferroelectricity in Mn-doped HfO_2(111) epitaxial thin films through controlled doping and substrate orientation

Jiayi Gu(顾嘉仪), Haiyi Zhang(张海义), Weijin Pan(潘炜进), Haifeng Bu(卜海峰), Zhijian Shen(沈志健), Shengchun Shen(沈胜春), Yuewei Yin(殷月伟), and Xiaoguang Li(李晓光)

Citation: Chin. Phys. B, 2025, 34 (**8**): 087701. DOI: 10.1088/1674-1056/add1bc
http://cpb.iphy.ac.cn; http://iopscience.iop.org/cpb

What follows is a list of articles you may be interested in

Molecular dynamics simulations of ferroelectricity in P(VDF-TrFE)

Mengyuan Tang(唐梦圆), Chuhan Tang(唐楚涵), Sheng-Yi Xie(谢声意), and Fuxiang Li(李福祥)
Chin. Phys. B, 2025, 34 (**6**): 067701. DOI: 10.1088/1674-1056/adbbc1

Manipulating optical and electronic properties through interfacial ferroelectricity

Yulu Liu(刘钰璐), Gan Liu(刘敢), and Xiaoxiang Xi(奚啸翔)
Chin. Phys. B, 2025, 34 (**1**): 017701. DOI: 10.1088/1674-1056/ad9456

Observing ferroelastic switching in $Hf_{0.5}Zr_{0.5}O_2$ thin film

Zhao Guan(关赵), Tao Wang(王陶), Yunzhe Zheng(郑赟喆), Yue Peng(彭悦), Luqi Wei(魏鹿奇), Yuke Zhang(张宇科), Abliz Mattursun(阿卜力孜 cdot 麦提图尔荪), Jiahao Huang(黄家豪), Wen-Yi Tong(童文旖), Genquan Han(韩根全), Binbin Chen(陈斌斌), Ping-Hua Xiang(向平华), Chun-Gang Duan(段纯刚), and Ni Zhong(钟妮)
Chin. Phys. B, 2024, 33 (**6**): 067701. DOI: 10.1088/1674-1056/ad362f

Impact of annealing temperature on the ferroelectric properties of $W/Hf_{0.5}Zr_{0.5}O_2/W$ capacitor

Dao Wang(王岛), Yan Zhang(张岩), Yongbin Guo(郭永斌), Zhenzhen Shang(尚真真), Fangjian Fu(符方健), and Xubing Lu(陆旭兵)
Chin. Phys. B, 2023, 32 (**9**): 097701. DOI: 10.1088/1674-1056/aca9c6

Ferroelectricity induced by the absorption of water molecules on double helix SnIP

Dan Liu(刘聃), Ran Wei(魏冉), Lin Han(韩琳), Chen Zhu(朱琛), and Shuai Dong(董帅)
Chin. Phys. B, 2023, 32 (**3**): 037701. DOI: 10.1088/1674-1056/ac7f8e

---

Improved ferroelectricity in Mn-doped HfO_2 (111) epitaxial thin films through controlled doping and substrate orientation

Jiayi Gu(顾嘉仪)[1], Haiyi Zhang(张海义)[1], Weijin Pan(潘炜进)[1], Haifeng Bu(卜海峰)[1], Zhijian Shen(沈志健)[1], Shengchun Shen(沈胜春)[1,†], Yuewei Yin(殷月伟)[1,‡], and Xiaoguang Li(李晓光)[1,2]

[1] *Hefei National Research Center for Physical Sciences at the Microscale, Department of Physics and CAS Key Laboratory of Strongly Coupled Quantum Matter Physics, University of Science and Technology of China, Hefei* 230026, *China*

[2] *Collaborative Innovation Center of Advanced Microstructures, Nanjing University, Nanjing* 210093, *China*

(Received 3 March 2025; revised manuscript received 17 April 2025; accepted manuscript online 29 April 2025)

Doped HfO_2 as an emerging ferroelectric material, holds considerable promise for non-volatile memory applications. Epitaxial growth of doped HfO_2 thin films is widely adopted as an effective technique for revealing the intrinsic ferroelectric properties. In this study, based on systematic structural, chemical and electrical investigations, the influences of Mn doping and substrate orientation on ferroelectric properties of Mn-doped HfO_2 epitaxial thin films are investigated. The results demonstrate that Mn-doped HfO_2 thin films with orthorhombic phase can be epitaxially grown along [111] out-of-plane direction on both $SrTiO_3$ (001) and (110) substrates, and 10% Mn-doping significantly stabilizes the orthorhombic polar phase and enhances the ferroelectric polarization. Interestingly, compared to the films on $SrTiO_3$ (001) substrate, the better crystallinity and reduction of oxygen vacancy amount in Mn-doped HfO_2 films grown on the $SrTiO_3$ (110) substrate are observed, which enhance the remanent polarization and reduce the coercive field. It provides an effective approach for the controllable regulation of defects and the enhancement of intrinsic ferroelectricity in HfO_2-based materials.

Keywords: HfO_2-based ferroelectric, substrate orientation, ferroelectricity, defects

PACS: 77.84.–s, 77.55.fp, 77.80.–e

DOI: 10.1088/1674-1056/add1bc **CSTR:** 32038.14.CPB.add1bc

1. Introduction

Hafnium dioxide (HfO_2), a notable transition metal oxide, has been extensively utilized as high dielectric materials in advanced semiconductor devices. Its wide bandgap ($\sim$ 5.3 eV–5.7 eV) and high dielectric constant ($\sim$ 20–40) make it particularly valuable for these applications.[1–3] As device dimensions continue to shrink, HfO_2 offers advantages that silicon dioxide (SiO_2) cannot match.[4] Since 2011, the reported ferroelectricity of doped-HfO_2 thin films gained significant attention.[5] Unlike the traditional perovskite ferroelectric materials, HfO_2-based films are compatible with silicon and can sustain excellent ferroelectric performance at thicknesses of less than 10 nm. These characteristics highlight their promising potential for use in high-density non-volatile ferroelectric memory devices.[6,7]

The ferroelectricity of HfO_2 originates from its metastable polar orthorhombic (O) phase with a non-centrosymmetric space group ($Pca2_1$).[8] Additionally, the recently discovered rhombohedral (R) phase in epitaxial films also exhibits polarity, which is stabilized by the combined effects of strain and size.[9–11] In contrast, the high-temperature tetragonal and cubic phases, as well as the room-temperature monoclinic phase, are typically non-polar.[12] Therefore, stabilizing the O-phase is crucial. Various methods to achieve this include doping,[13–15] stress,[16,17] and interface effects.[18] Doping, as one of the most common methods to tune ferroelectricity of HfO_2, has been studied based on various elements, such as Zr,[19] La,[20] Gd,[21] Al,[22] and Si,[23] which is beneficial to improve ferroelectric properties.[24]

Besides intrinsic doping, oxygen vacancies are particularly prominent and are typically affected by factors such as doping type, thermal treatment, and film thickness.[25] Both experimental and theoretical studies have demonstrated that suitable doping can activate oxygen vacancies and stabilize the ferroelectric phase, thereby enhancing ferroelectric performance.[26,27] However, the agglomeration of excessive oxygen vacancies will pin domain walls, resulting in detrimental effects on ferroelectric polarization switching, endurance, and retention.[28] Therefore, the effective control and optimization of these defects are essential for improving device performance.

Epitaxial growth of HfO_2 thin films is frequently employed to investigate intrinsic ferroelectricity due to the controllable phase structures and strain manipulation capabilities. It has been found that the buffer layer of $La_{0.67}Sr_{0.33}MnO_3$ (LSMO) can effectively stabilize the O phase in epitaxial HfO_2-based films, which was attributed to the MnO_2-terminated LSMO.[29] In addition, compared to dopants of

†Corresponding author. E-mail: scshen@ustc.edu.cn

‡Corresponding author. E-mail: yyw@ustc.edu.cn

© 2025 Chinese Physical Society and IOP Publishing Ltd. All rights, including for text and data mining, AI training, and similar technologies, are reserved.

Zr^{4+} and La^{3+}, Mn ions exhibit multiple valence states, such as Mn^{4+} and Mn^{2+}, which may provide enhanced flexibility to tune the generation and distribution of oxygen vacancies. These indicate that Mn doping into HfO_2 epitaxial film would be important, but the relevant study is rare.[30] The crystal orientation of the substrate can significantly influence the epitaxial growth of HfO_2 thin films, thereby tuning the stability of the ferroelectric orthorhombic phase.[31] Therefore, investigating the combined effects of Mn doping and substrate orientation on HfO_2-based thin films is of significant importance for further understanding their ferroelectric properties.

In this work, epitaxial (111)-oriented $Hf_{1-x}Mn_xO_2$ films with O phase were grown on (110)- and (001)-oriented $SrTiO_3$ (STO) substrates by pulsed laser deposition. The evolution of structural, chemical, and ferroelectric properties of the HfO_2 films with different Mn concentrations were investigated. It was found that compared to $Hf_{1-x}Mn_xO_2$ films grown on (001)-oriented STO substrates, $Hf_{1-x}Mn_xO_2$ films grown on (110)-oriented STO substrates exhibit better crystallinity and fewer oxygen vacancies, leading to lower E_c and higher P_r values. These results further reveal the detrimental effect of excessive amount of oxygen vacancies on the ferroelectricity, and provide a strategy to tune the oxygen vacancies.

2. Experiments

Firstly, HfO_2 targets with different Mn doping concentrations were sintered using spark plasma sintering (SPS) system. Next, bilayer films of LSMO ($\sim$ 20 nm in thickness) and $Hf_{1-x}Mn_xO_2$ were deposited on both (001)- and (110)-oriented STO substrates using pulsed laser deposition (PLD) system. The LSMO bottom electrode layer was deposited at 650 °C under an oxygen atmosphere of 20 Pa with a laser frequency of 5 Hz and laser energy density of 1.3 J/cm^2. Subsequently, epitaxial $Hf_{1-x}Mn_xO_2$ films were grown on LSMO layer at 825 °C under an oxygen pressure of 13 Pa with a laser frequency of 2 Hz. Finally, the films were cooled to room temperature at a rate of 8 °C/min in 1000-Pa oxygen. The circular top electrode (Pt) was prepared using magnetron sputtering and lift-off lithography.

The x-ray diffraction (XRD) with Cu $K_{\alpha 1}$ radiation was used to characterize the crystal structure of the epitaxial films. Moreover, the thicknesses of $Hf_{1-x}Mn_xO_2$ and LSMO films were obtained by x-ray reflectivity (XRR). Cross-sectional high-angle annular dark-field scanning transmission electron microscopy (HAADF-STEM) was utilized to investigate the lattice structures of the films. The switchable ferroelectric domains were investigated using piezoresponse force microscopy (PFM). The x-ray absorption spectroscopy (XAS) was performed at the Hefei Light Source (National Synchrotron Radiation Laboratory), utilizing the x-ray magnetic circular dichroism (XMCD) experimental station. The measurements were conducted with a spot size of 0.5 mm×1 mm and an energy range of 50 eV–1000 eV. The x-ray photoelectron spectroscopy (XPS, Kratos AXIS SUPRA+) were implemented with the monochromatized x-ray source Al K_α (1486.6 eV). The measured binding energy were calibrated using the C 1s peak at 284.8 eV. The macroscopic ferroelectric properties of the Pt/$Hf_{1-x}Mn_xO_2$/LSMO/STO capacitors were measured using Keithley 4200A-SCS Parameter Analyzer, using the PUND (Positive-Up Negative-Down) mode at 10-kHz triangular electric pulse.

3. Results and discussion

The XRD θ–2θ scans of $Hf_{1-x}Mn_xO_2$ ($x = 0$, 0.05, 0.1, 0.15) films with a thickness of 10 nm grown under the same conditions on (001)- and (110)-oriented LSMO/STO substrates are shown in Figs. 1(a) and 1(b), respectively. The $Hf_{1-x}Mn_xO_2$ films predominantly exhibit epitaxial growth along the O-(111) direction ($2\theta \sim 30.1°$), with additional diffraction peaks for M-($\bar{1}11$) ($2\theta \sim 28.4°$) and O/M-(002) ($2\theta \sim 34.3°$).[32] The intensity of the M-phase peaks first decreases and then increases with increasing Mn doping content, and the similar trend is found for $Hf_{1-x}Mn_xO_2$ films grown on STO substrates with both (001)- and (110)-orientations. Notably, the M-phase vanishes, and the clear Laue oscillations are observed around the O-(111) peak in films with $x = 0.1$. According to the fitting of Laue fringes (Fig. S1 in supporting information), the thickness of $Hf_{0.9}Mn_{0.1}O_2$ films is $\sim$ 10 nm. An Mn doping concentration of nearly 10% is more favorable for stabilizing the O-phase.

The epitaxial growth of $Hf_{0.9}Mn_{0.1}O_2$ films along O-(111) were also evidenced by HAADF-STEM images as shown in Fig. S2 in the supporting information. The identical epitaxial crystal structures of $Hf_{0.9}Mn_{0.1}O_2$ on (110)- and (001)-oriented STO substrates at the same doping concentration indicate that the primary factors influencing the stabilization of the O-phase in $Hf_{1-x}Mn_xO_2$ films are the doping effects.

Figures 1(c) and S3 display rocking curves of the $Hf_{1-x}Mn_xO_2$ films with different doping concentrations on STO (001) and STO (110) substrates. The rocking curves of $Hf_{1-x}Mn_xO_2$ films typically consists of two components: a sharp peak at the top, signifying regular two-dimensional (2D) growth, and a broad peak at the bottom corresponding to irregular three-dimensional (3D) growth.[9] The crystallinity of films can be characterized by the ratio of the sharp/broad peak.[10] Figure 1(d) exhibits the variation in the sharp/broad peak ratio with different doping concentrations. The crystallinity peaks at a doping level of $x = 0.1$, which may be associated with the disappearance of the M-($\bar{1}11$) peak. With purer O phase, defects, such as dislocations, likely forming at

the boundaries between different phases, will be less, leading to an increase in crystallinity. Notably, for all doping concentrations, $Hf_{1-x}Mn_xO_2$ films grown on STO (110) exhibit significantly higher crystallinity compared to those grown on STO (001).

It is well established that the substrate symmetry significantly influences both the single-crystallinity and the ferroelectric phase fraction of HfO_2 thin films.[33] In particular, the 4-fold symmetry of an STO (001) surface differs markedly from the 2-fold symmetry of an STO (110) surface, leading to distinct domain-matching mechanisms in HfO_2 films.[34] Figures 1(e) and 1(f) show XRD Φ-scan pattern of $Hf_{0.9}Mn_{0.1}O_2$ films at $\chi = 71°$. On the STO (001) substrate, twelve diffraction peaks are observed, each separated by $\Phi = 30°$, indicating the presence of crystal variants in O-(111) $Hf_{0.9}Mn_{0.1}O_2$ (3-fold symmetric surface) that are rotated by 90° relative to one another. In contrast, for O-(111) $Hf_{0.9}Mn_{0.1}O_2$ grown on STO (110), six pairs of diffraction peaks separated by 60° are observed, arising from the interplay between the 2-fold symmetry of the substrate and the 3-fold symmetry inherent to the $Hf_{0.9}Mn_{0.1}O_2$ films. This results in the rotation of 2 domains by 180° with respect to the out-of-plane [111] direction. The appearance of double peaks suggests a degree of domain misalignment, and this kind of the epitaxial structure can effectively reduce the misfit.[31,35] In comparison to the $Hf_{0.9}Mn_{0.1}O_2$ (111)/LSMO (100), the $Hf_{0.9}Mn_{0.1}O_2$ (111)/LSMO (110) epitaxial structure is conducive to the reduction of structurally equivalent domains and defects, thereby enhancing crystallinity.

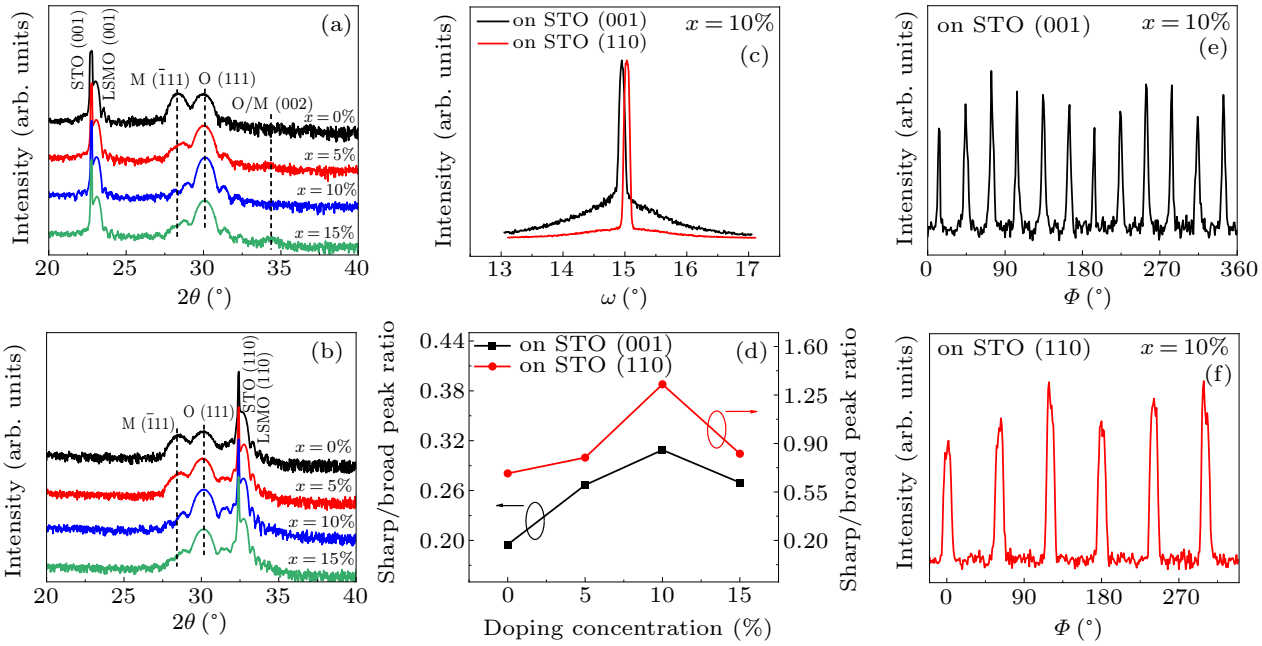


Fig. 1. XRD θ–2θ scans for $Hf_{1-x}Mn_xO_2$ films on (a) (001)- and (b) (110)-oriented LSMO/STO bilayers. (c) Rocking curves of $Hf_{0.9}Mn_{0.1}O_2$ films on STO (001) and STO (110). (d) Doping concentration-dependent sharp/broad peak ratio for $Hf_{1-x}Mn_xO_2$ film on STO (001) and STO (110). XRD Φ-scan pattern O-(111) reflections for $Hf_{0.9}Mn_{0.1}O_2$ films on (e) STO (001) and (f) STO (110).

Oxygen vacancies are often unavoidable in ferroelectric oxide layers and significantly impact various properties, including coercive field, wake-up, and breakdown characteristics.[36–38] To investigate the effect of different substrate orientations on the formation of oxygen vacancy (V_O) defects, XPS spectra were analyzed. Prior to measurement, the surface of the $Hf_{1-x}Mn_xO_2$ film was etched with Ar^+ ions at 1 keV for 15 seconds to eliminate the effects of adsorbed species such as oxygen and water from the air.[39] A charge calibration was performed using the C 1s peak (284.8 eV).[40] Figures 2(a), 2(b) and S6 illustrate the details of the O 1s spectra deconvoluted into two peaks: one corresponding to the lattice oxygen peak associated with the Hf–O bond, and the other representing the non-lattice oxygen/oxygen vacancy peak.[41] Figures 2(c), 2(d) and S7 show the Hf 4f spectra with the binding energies of ∼ 16.6 eV and ∼ 18.3 eV corresponding to Hf^{4+} $4f_{7/2}$ and Hf^{4+} $4f_{5/2}$, and ∼ 16.1 eV and ∼ 17.8 eV corresponding to Hf^{x+} $4f_{7/2}$ and Hf^{x+} $4f_{5/2}$, respectively. It is evident that the oxygen vacancy and Hf^{x+} concentration in $Hf_{1-x}Mn_xO_2$ films grown on STO (110) substrates is significantly lower than that in films grown on STO (001) substrates across all doping concentrations (Figs. 2(e) and 2(f)). This is attributed to the high crystallinity of the STO (110)-grown films, which inhibits the formation of defects. Moreover, the changes in the binding energies of O 1s and Hf 4f, show the same trend: their binding energies shift to higher energies as Mn content is increased from 0% to 10%, and subsequently shift back to lower energies at 15%-Mn content, which is attributed to alterations in the chemical environments of Hf and O, as well as the transformation of the $Hf_{1-x}Mn_xO_2$ crystal structure caused by variations in doping levels. Similar trends were observed in the Y-doped HfO_2 (HYO) films.[42]

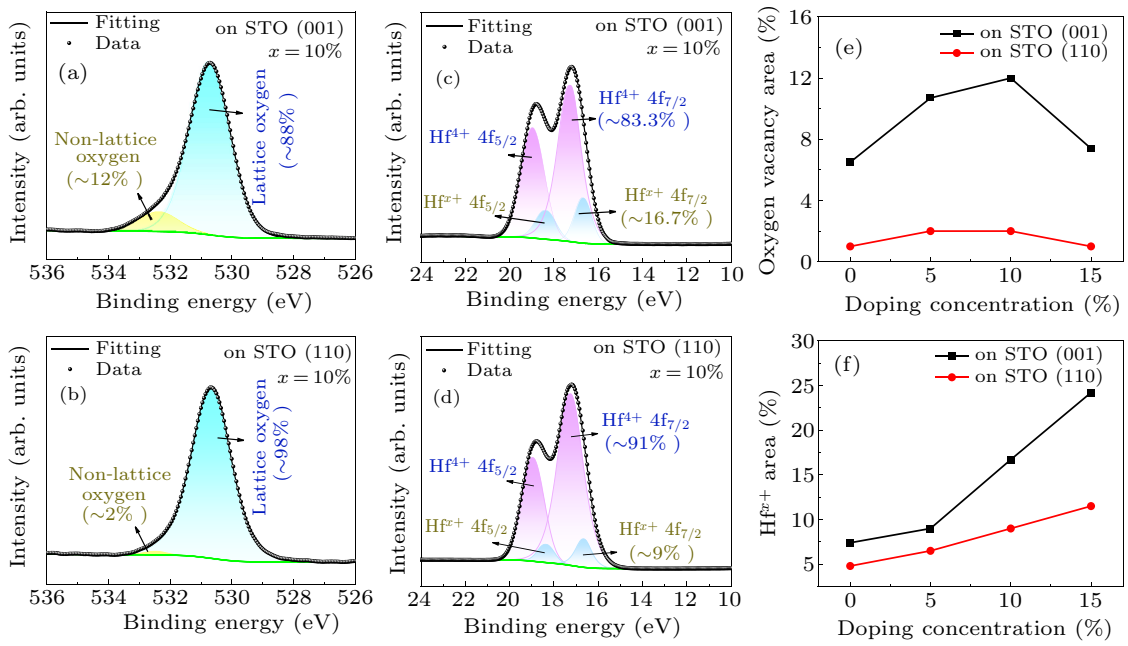


Fig. 2. The O 1s and Hf 4f XPS spectra of 10-nm thick $Hf_{0.9}Mn_{0.1}O_2$ films on [(a), (c)] STO (001) and [(b), (d)] STO (110). The estimated content of (e) oxygen vacancy and (f) Hf^{x+} for $Hf_{1-x}Mn_xO_2$ films on STO (001) and STO (110).

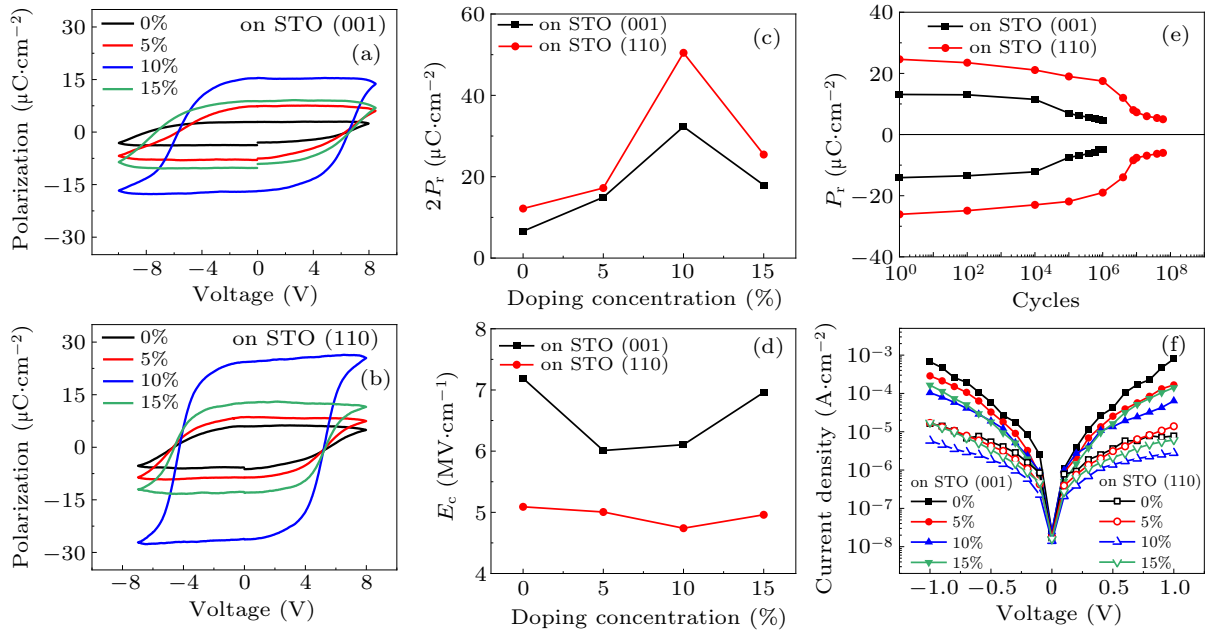


Fig. 3. The *P*–*V* loops with different doping concentrations of $Hf_{1-x}Mn_xO_2$ films on (a) STO (001) and (b) STO (110). (c) $2P_r$ and (d) E_c dependence on different doping concentrations of $Hf_{1-x}Mn_xO_2$ films on STO (001) and STO (110). (e) Endurance measurements of $Hf_{0.9}Mn_{0.1}O_2$ films. (f) Leakage current curves of $Hf_{1-x}Mn_xO_2$ films grown on STO (001) and STO (110).

The ferroelectric characterization of $Hf_{1-x}Mn_xO_2$ films including the measurement of polarization–voltage (*P*–*V*) loops in PUND mode and corresponding ferroelectric switching current are shown in Figs. 3(a), 3(b), and S9. For $Hf_{1-x}Mn_xO_2$ films on (001)-STO and (110)-STO substrates, pure HfO_2 exhibits modest remanent polarization (P_r) with weak ferroelectric switching peaks, indicating relatively weak ferroelectricity, which is associated with the presence of the M-phase. The ferroelectricity of the $Hf_{1-x}Mn_xO_2$ films was significantly enhanced through the doping of Mn ions, and the P_r values initially increased with Mn content and then decreased at higher doping levels. The maximum P_r value was attained in the film with $x = 0.1$. The ferroelectricity $Hf_{0.9}Mn_{0.1}O_2$ films was also confirmed by PFM hysteresis loops in Fig. S10. Combined with XRD results, it suggests that an Mn concentration of 10% is optimal for stabilizing the ferroelectric O phase and achieving improved ferroelectricity, regardless of whether the substrate is STO (001) or STO (110). The concentration is higher than the 3% optimal concentration observed in epitaxial La-HfO_2 films, which may be attributed to the differences in the size and chemical properties of the various elements involved.[26] In comparison to the films on

STO (110) substrate, the ferroelectric *P*–*V* hysteresis loops of the $Hf_{1-x}Mn_xO_2$ films grown on the STO (001) substrate appear more "rounded", with more "blunted" current peaks and lower P_r values with equivalent Mn doping levels, which can be attributed to the elevated defect density. Figures 3(c) and 3(d) summarizes $2P_r$ values and coercive fields (E_c) of $Hf_{1-x}Mn_xO_2$ films on both substrates. Compared to the films on STO (110) substrate, $Hf_{1-x}Mn_xO_2$ films grown on STO (001) substrates exhibit lower $2P_r$ values and higher E_c, which is attributed to the pinning of ferroelectric domains caused by an excess of oxygen vacancies.[24] This further highlights the impact of defects on the ferroelectric domain switching behavior.

Besides, as shown in Fig. 3(e), the endurance properties of $Hf_{0.9}Mn_{0.1}O_2$ thin films grown on STO (001) and (110) substrates were measured. Compared to the film on STO (001), the $Hf_{0.9}Mn_{0.1}O_2$ film on STO (110) with superior crystallinity and low defect content shows better endurance performance. The leakage current curves of $Hf_{1-x}Mn_xO_2$ films on STO (001) and STO (110) are shown in Fig. 3(f). The films grown on STO (110) show lower leakage current.

Figures 4(a) and 4(b) illustrate the variation of ferroelectric properties of $Hf_{0.9}Mn_{0.1}O_2$ films on STO (001) and STO (110) in the temperature range of 77 K–300 K. Both the P_r values and E_c decrease gradually with decreasing temperature until 77 K, which is the same as the previous reports about the trend of epitaxial HYO with temperature.[10] In contrast, the P_r values and E_c of polycrystalline HZO films and conventional chalcogenide ferroelectric films decrease with increasing temperature.[43,44] For epitaxial $Hf_{0.9}Mn_{0.1}O_2$, the ferroelectric behavior at room temperature is affected by non-intrinsic factors such as oxygen vacancy migration. As the temperature declines, the thermal movement of oxygen vacancies is markedly diminished and ultimately arrested. At this point, the *P*–*V* loops exemplify the intrinsic ferroelectric characteristics. Figures 4(c) and 4(d) summarize the temperature dependence of the P_r values and E_c for $Hf_{0.9}Mn_{0.1}O_2$ films. As the temperature is reduced from room temperature to 77 K, a 36% decrease in P_r values is observed for $Hf_{0.9}Mn_{0.1}O_2$ films on STO (001), accompanied by a 6.8% decrease in E_c. In contrast, the P_r values and E_c for the films on STO (110) exhibit a comparatively minor decrease of 11% and 3.3%, respectively. These observations provide further evidence to support that $Hf_{0.9}Mn_{0.1}O_2$ films on STO (110) contain a reduced number of oxygen vacancies than STO (001), a conclusion that is consistent with the results observed through XPS analysis.

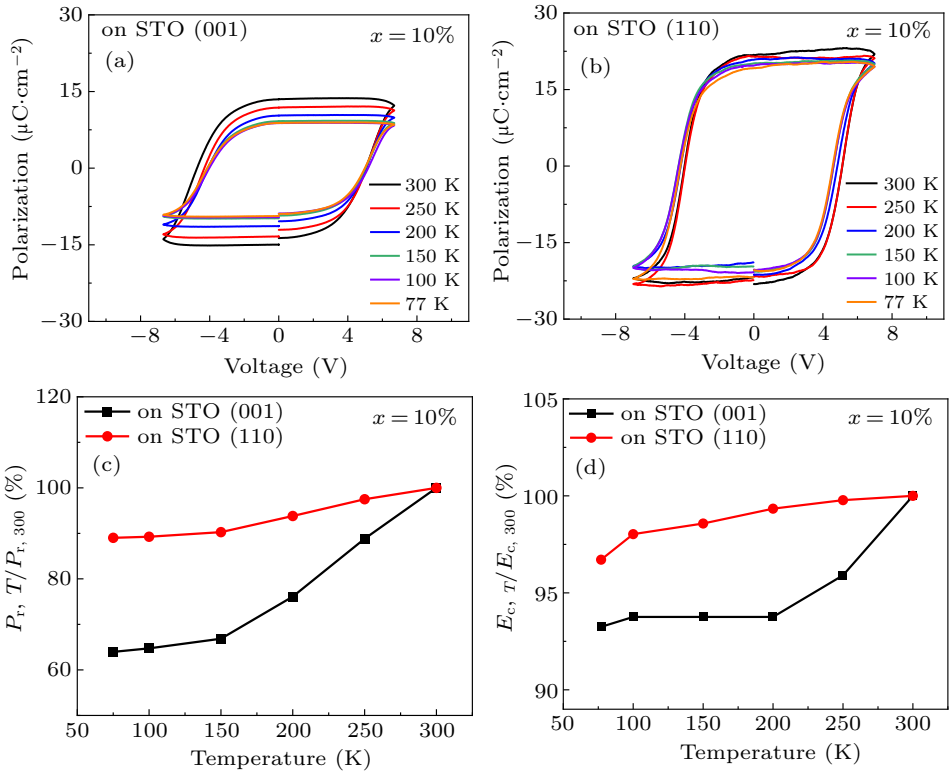


Fig. 4. Temperature dependence of ferroelectricity in $Hf_{0.9}Mn_{0.1}O_2$ films on (a) STO (001) and (b) STO (110). (c) P_r and (d) E_c dependence on temperature of $Hf_{0.9}Mn_{0.1}O_2$ films on STO (001) and STO (110).

4. Conclusion

In conclusion, we used the PLD method to deposit high-quality epitaxial single-crystal $Hf_{1-x}Mn_xO_2$ thin films. The most favourable O-phase stabilisation and robust ferroelectric properties were observed at a 10%-Mn doping concentration on (001)- and (110)-oriented STO substrates. Notably, compared to (001)-oriented STO substrates, $Hf_{1-x}Mn_xO_2$ films

grown on (110)-oriented STO substrates exhibited higher crystallinity and fewer oxygen vacancies, leading to lower E_c and higher P_r values. This work not only elucidates the crucial role of substrate orientation in controlling oxygen vacancy defects but also provides a strategy for defect engineering to optimize the performance of HfO_2 ferroelectric materials.

Supplementary material

See supplementary material for the additional structures, XPS results, and ferroelectric and dielectric properties of epitaxial $Hf_{1-x}Mn_xO_2$ films.

Acknowledgements

Project supported by the National Natural Science Foundation of China (Grant Nos. 52125204, 52250281, 52422209, 92163210, and U21A2066) and the National Key Research and Development Program of China (Grant Nos. 2024YFA1208601, 2022YFB3807602, and 2022YFB3807604). The authors would like to acknowledge Beamlines MCD-A at National Synchrotron Radiation Laboratory (Hefei, China) for the synchrotron beamtime.

References

[1] Li W F, Liu T W, Yang Z M, Wang L W and Liu Y Y 2025 *Chin. Phys. Lett.* **42** 017302
[2] Park M H, Lee Y H, Mikolajick T, Schroeder U and Hwang C S 2018 *MRS Commun.* **8** 795
[3] Kim S J, Mohan J, Summerfelt S R and Kim J 2019 *JOM* **71** 246
[4] Zhu H, Tang C, Fonseca L R C and Ramprasad R 2012 *J. Mater. Sci.* **47** 7399
[5] Böscke T S, Müller J, Bräuhaus D, Schröder U and Böttger U 2011 *Appl. Phys. Lett.* **99** 102903
[6] Ramaswamy N, Calderoni A, Zahurak J, Servalli G, Chavan A, Chhajed S, Balakrishnan M, Fischer M, Hollander M, Ettisserry D P, Liao A, Karda K, Jerry M, Mariani M, Visconti A, Cook B R, Cook B D, Mills D, Torsi A, Mouli C, Byers E, Helm M, Pawlowski S, Shiratake S and Chandrasekaran N 2023 *IEDM* p. 1
[7] Wang D, Zhang Y, Guo Y B, Shang Z Z, Fu F J and Lu X B 2023 *Chin. Phys. B* **32** 097701
[8] Kisi E H, Howard C J and Hill R J 1989 *J. Am. Ceram.* **72** 1757
[9] Jiao P, Cheng H, Li J, Chen H, Liu Z, Xi Z, Ding W, Ma X, Wang J, Zheng N, Nie Y, Deng Y, Bellaiche L, Yang Y and Wu D 2023 *Appl. Phys. Rev.* **10** 031417
[10] Yun Y, Buragohain P, Li M, Ahmadi Z, Zhang Y Z, Li X, Wang H H, Li J, Lu P, Tao L L, Wang H Y, Shield J E, Tsymbal E Y, Gruverman A and Xu X S 2022 *Nat. Mater.* **21** 903
[11] Schroeder U, Park M H, Mikolajick T and Hwang C S 2022 *Nat. Rev. Mater.* **7** 653
[12] Wei Y F, Nukala P, Salverda M, Matzen S, Zhao H J, Momand J, Everhardt A S, Agnus G, Blake G R, Lecoeur P, Kooi B J, Iñiguez J, Dkhil B and Noheda B 2018 *Nat. Mater.* **17** 1095
[13] Gao R L, Liu C, Shi B W, Li Y C, Luo B, Chen R, Ouyang W B, Gao H, Hu S B, Wang Y, Li D D and Ren W 2024 *Chin. Phys. Lett.* **41** 087701
[14] Song T, Tan H, Dix N, Moalla R, Lyu J, Saint-Girons G, Bachelet R, Sánchez F and Fina I 2021 *ACS Appl. Electron. Mater.* **3** 2106
[15] Song T, Tan H, Bachelet R, Saint-Girons G, Fina I and Sánchez F 2021 *ACS Appl. Electron. Mater.* **3** 4809
[16] Liu K, Liu K, Zhang X C, Fang J, Jin F, Wu W B, Ma C and Wang L F 2024 *Chin. Phys. Lett.* **41** 117701
[17] Song T F, Lenzi V, Silva J P B, Marques L, Fina I and Sánchez F 2023 *Appl. Phys. Rev.* **10** 041415
[18] Estandía S, Gàzquez J, Varela M, Dix N, Qian M D, Solanas R, Fina I and Sánchez F 2021 *J. Mater. Chem. C* **9** 3486
[19] Zhou X, Sun H Y, Li J C, Du X Z, Wang H, Luo Z, Wang Z J, Lin Y, Shen S C, Yin Y W and Li X G 2024 *J. Materiomics* **10** 210
[20] Xu Z, Lu L, Xu J, Zheng W, Yu Y, Ding C, Wang S, Chen F, Tang M, Lu C and Wen Z 2022 *Appl. Phys. Lett.* **120** 133504
[21] Cavalieri M, O'Connor É, Gastaldi C, Stolichnov I and Ionescu A M 2020 *ACS Appl. Electron. Mater.* **2** 1752
[22] Yao L, Liu X, Cheng Y and Xiao B 2021 *Nanotechnology* **32** 215708
[23] Park M H, Chung C C, Schenk T, Richter C, Hoffmann M, Wirth S, Jones J L, Mikolajick T and Schroeder U 2018 *Adv. Electron. Mater.* **4** 1700489
[24] Zhou C, Ma L Y, Feng Y P, Kuo C Y, Ku Y C, Liu C E, Cheng X L, Li J X, Si Y Y, Huang H L, Huang Y, Zhao H J, Chang C F, Das S, Liu S and Chen Z H 2024 *Nat. Commun.* **15** 2893
[25] Chouprik A, Negrov D, Tsymbal E Y and Zenkevich A 2021 *Nanoscale* **13** 11635
[26] Shen Z, Liao L, Zhou Y, Xiong K, Zeng J, Wang X, Chen Y, Liu J, Guo T, Zhang S, Lin T, Shen H, Meng X, Wang Y, Cheng Y, Yang J, Chen P, Wang L, Bai X, Chu J and Wang J 2022 *Appl. Phys. Lett.* **120** 162904
[27] Kaiser N, Song Y J, Vogel T, Piros E, Kim T, Schreyer P, Petzold S, Valenti R and Alff L 2023 *ACS Appl. Electron. Mater.* **5** 754
[28] Lee J, Yang K, Kwon J Y, Kim J E, Han D I, Lee D H, Yoon J H and Park M H 2023 *Nano Convergence* **10** 55
[29] Shi S, Xi H, Cao T, Lin W, Liu Z, Niu J, Lan D, Zhou C, Cao J, Su H, Zhao T, Yang P, Zhu Y, Yan X, Tsymbal E Y, Tian H and Chen J 2023 *Nat. Commun.* **14** 1780
[30] Guo J, Tao L, Xu X, Hou L, Nan C W, Du S, Chen C and Ma J 2024 *Adv. Mater.* **36** 2406038
[31] De A, Jung M H, Kim Y H, Bae S B, Jeong S G, Oh J Y, Choi Y, Lee H, Kim Y, Choi T, Kim Y M, Yang S M, Jeong H Y and Choi W S 2024 *ACS Appl. Mater. Interfaces* **16** 27532
[32] Song T F, Estandía S, Tan H, Dix N, Gàzquez J, Fina I and Sánchez F 2022 *Adv. Electron. Mater.* **8** 2100420
[33] Liu K, Jin F, Zhou L, Liu K, Fang J, Lu J, Ma C, Wang L and Wu W 2024 *ACS Appl. Mater. Interfaces* **16** 61239
[34] Song T, Tan H, Estandia S, Gazquez J, Gich M, Dix N, Fina I and Sanchez F 2022 *Nanoscale* **14** 2337
[35] Jiao P J, Li J Y, Xi Z N, Zhang X Y, Wang J, Yang Y R, Deng Y and Wu D 2021 *Appl. Phys. Lett.* **119** 252901
[36] Zhang H Y, Tu Y C, Wang Z J, Zhou X, Wang Y C, Du X Z, Shen S C, Yin Y W and Li X G 2024 *J. Phys. D: Appl. Phys.* **57** 365305
[37] Jiang P F, Luo Q, Xu X X, Gong T C, Yuan P, Wang Y, Gao Z M, Wei W, Tai L and Lv H B 2021 *Adv. Electron. Mater.* **7** 2000728
[38] Choi Y, Shin J, Moon S, Min J, Han C and Shin C 2023 *Nanotechnology* **34** 185203
[39] Zhang X Y, Han J, Peng D C, Ruan Y J, Wu W Y, Wuu D S, Huang C J, Lien S Y and Zhu W Z 2022 *Nanomaterials* **12** 3890
[40] Zhang Y, Xu J, Zhou D Y, Wang H H, Lu W Q and Choi C K 2018 *Chin. Phys. B* **27** 048103
[41] Luo X G, Li Y, Yang H, Liang Y L, He K Y, Sun W H, Lin H H, Yao S D, Lu X, Wan L Y and Feng Z C 2018 *Crystals* **8** 248
[42] Nand M, Tripathi S, Rajput P, Kumar M, Kumar Y, Mandal S K, Urkude R, Gupta M, Dawar A, Ojha S, Rai S K and Jha S N 2022 *J. Alloys Compd.* **928** 167099
[43] Wang H, Guan Z Y, Li J C, Luo Z, Du X Z, Wang Z J, Zhao H Y, Shen S C, Yin Y W and Li X G 2024 *Adv. Mater.* **36** 2211305
[44] Yang J, Meng X J, Shen M R, Gao C, Sun J L and Chu J H 2008 *Appl. Phys. Lett.* **93** 092908